Impacts of mesoscale activity on the water masses and circulation in the Coral Sea.

L. Rousselet,[1] A.M. Doglioli,[1] C. Maes,[2] B. Blanke,[2] and A. Petrenko[1]

Corresponding author: L. Rousselet, MIO - Institut Méditerranéen d'Océanologie, Bureau 155, 1er étage, Campus de Luminy-Case 901, 13288 MARSEILLE cedex 9, France. (louise.rousselet@mio.osupytheas.fr)

[1]Aix Marseille Université, Université de Toulon, CNRS, IRD, Mediterranean Institute of Oceanography (MIO), Marseille, France

[2]Laboratoire d'Océanographie Physique et Spatiale (LOPS), CNRS, Ifremer, IRD, UBO, Brest, France

Key Points.

Eddy circulation, water masses mixing, jets connection

Abstract. The climatological vision of the circulation within the Coral Sea is today well established with the westward circulation of two main jets, the North Caledonian Jet (NCJ) and the North Vanuatu Jet (NVJ) as a consequence of the separation of the South Equatorial Current (SEC) on the islands of New Caledonia, Vanuatu and Fiji. Each jet has its own dynamic and transports different water masses across the Coral Sea. The influence of mesoscale activity on mean flow and on water mass exchanges is not yet fully explored in this region of intense activity. Our study relies on the analysis of *in situ*, satellite and numerical data. Indeed we first use *in situ* data from the Bifurcation cruise and from an Argo float, jointly with satellite-derived velocities, to study the eddy influence on the Coral Sea dynamics. We identify an anticyclonic eddy as participating in the transport of NVJ-like water masses into the theoretical pathway of NCJ waters. This transfer from the NVJ to the NCJ is confirmed over the long-term by a Lagrangian analysis. In particular, this numerical analysis shows that anticyclonic eddies can contribute up to 70% to 90% of the overall eddy transfer between those seemingly independent jets. Finally, transports calculated using S-ADCP measurements (0-500 m) show an eddy-induced sensitivity that can reach up to 15 Sv, i.e, the order of the transport of the jets.

1. Introduction

The circulation within the Coral Sea is presently well established from a climatological point of view. As the South Equatorial Current (SEC) approaches the Coral Sea from the east, it hits the islands of New Caledonia, Vanuatu and Fiji. This results in its separation into two main jets entering the Coral Sea: the North Vanuatu Jet (NVJ) between the Solomon Islands and Vanuatu (generally located between 11° S and 15° S) and the North Caledonian Jet (NCJ) between Vanuatu and New Caledonia flowing approximately at 18° S [*Webb*, 2000; *Sokolov and Rintoul*, 2000; *Ganachaud et al.*, 2008; *Qiu et al.*, 2009; *Kessler and Cravatte*, 2013a; *Ganachaud et al.*, 2014]. These jets cross the Coral Sea towards the Australian shelf where they contribute to the formation of western boundary currents: the Gulf of Papua Current flowing north towards the Solomon Sea and the East Australian Current flowing south towards the Tasman Sea [*Ridgway and Dunn*, 2003; *Choukroun et al.*, 2010; *Burrage et al.*, 2012].

Despite their similar origins and pathways, the NVJ and the NCJ present different characteristics in their journey to the western Pacific. The NCJ is rather narrow (∼100 km) and vertically thick (∼1000 m), transporting about 15 ± 5 Sv ($1\ \mathrm{Sv} = 10^6\ \mathrm{m^3\ s^{-1}}$) of Pacific central waters. On the contrary, the NVJ is wider (∼300 km) and shallower (∼500 m), with a larger transport (about 20 ± 5 Sv) [*Gourdeau et al.*, 2008; *Gasparin*, 2012; *Kessler and Cravatte*, 2013a]. Together, the NVJ and the NCJ represent almost the entire flow that enters the Coral Sea, which is estimated at 25 to 45 Sv, depending upon the various studies and methods used [*Ganachaud et al.*, 2014]. Calculation methods, seasonal and

interannual variabilities are often pointed out as sources of uncertainty in mass transport estimations, unlike mesoscale activity that has been hardly considered in previous studies.

High-resolution regional oceanic models confirm that the baroclinic flow entering the Coral Sea is strongly influenced by topography resulting with the NVJ and the NCJ [*Kessler and Gourdeau*, 2007; *Couvelard et al.*, 2008]. Model outputs also agree on the differences in vertical structure and transport between the westward jets [*Hristova et al.*, 2014]. The latter study and *Qiu et al.* [2009] also showed that barotropic instabilities of the NVJ and the NCJ are the cause of most of the Coral Sea mesoscale variability in both model and altimetry studies. The mesoscale activity is marked by a seasonal shift in the surface eddy population from small and intense eddies in late winter (August to October) to large and weak eddies from December to February. On the global scale, model outputs and altimetry analysis show that eddy activity is a significant feature of the Coral Sea dynamics and has to be considered as a structural component of the regional ocean dynamics, *Chelton et al.* [2007] estimating that oceanic eddies contribute to 50% of the variability over much of the World Ocean.

Moreover, the NVJ and the NCJ can clearly be distinguished one from the other by their different water masses. Even though the surface waters, called Tropical Surface Waters (TSW), remain rather fresh owing to high local precipitations [*Wyrtki*, 1962; *Sokolov and Rintoul*, 2000], they can be strongly influenced by waters below the surface mixed layer. *Gasparin et al.* [2014] focused on the different water masses of both jets at the entrance of the Coral Sea. According to their description, the NVJ thermocline waters are composed of the South Pacific Tropical Water North (SPTWN, $\sigma = 24{,}5$ kg m^{-3}) and the Pacific Equatorial Water (PEW, $\sigma = 26{,}3$ kg m^{-3}) that are both typical of an eastern

equatorial origin. The PEW is formed by convective sinking of surface salty waters, due to high evaporation, south of the equator and west of 170°W (between Polynesia and South America). After its journey across the South Pacific Ocean, the salinity of the PEW is detected between 0 and 500 m in the Coral Sea [*Emery*, 2001; *Tomczak and Godfrey*, 2013]. The NCJ thermocline waters are dominated by the South Pacific Tropical Water South (SPTWS, σ = 25,3 kg m^{-3}) and the Western South Pacific Central Water (WSPCW, σ = 26,3 kg m^{-3}), saltier and more oxygenated than the NVJ thermocline waters. The WSPCW is formed between Tasmania and New Zealand, in a region assumed to be restricted to west of 150°W and generally south of 15°S [*Tomczak and Hao*, 1989]. However heat and salt exchanges within the thermocline in the Coral Sea remain to be explored as *Gasparin* [2012] found a mixture of WSPCW at the entrance of the Solomon Sea. The transit of temperature and salinity anomalies at these depths may alter the mean structure of the equatorial thermocline which plays an important role in long-term variations of the tropical circulation (with time scales of 20 to 50 years). Below the main thermocline, the Antarctic Intermediate Water (AAIW) enters the Coral Sea between 400 and 1000 m. The AAIW is in general characterized by a salinity minimum and an oxygen maximum. After its journey across the South Pacific anticyclonic gyre, the AAIW is advected by the SEC in the deep part of the two jets [*Maes et al.*, 2007]. Because of sharp contrasts in physical properties, the pathways of the NVJ and the NCJ through the Coral Sea are generally assumed to be independent, but *Gasparin et al.* [2014] showed the presence of water mass mixing within the thermocline, between 13°S and 15°S, possibly caused by the recirculation of the two jets [*Qiu et al.*, 2009]. Indeed the barotropic

instability associated with the NVJ and NCJ circulation contributes to the meridional heat exchange and may induce water mass modifications.

The climatological vision of the circulation within the Coral Sea has evolved considerably since the pioneering work of *Webb* [2000] but the influence of the mesoscale activity, induced by the presence of numerous islands among other forcing, is yet not fully explored. Nonetheless some studies have underlined the role of westward-propagating eddies [*Chelton et al.*, 2007, 2011; *Rogé et al.*, 2015] to define the circulation in this area exposed to strong eddy variability [*Thompson and Veronis*, 1980; *Kessler and Cravatte*, 2013a]. Short-term signals such as the eddy contribution are known for aliasing mean circulation observations: across a meridional section sampled during the WOCE P11S cruise, *Kessler and Cravatte* [2013b] estimated that the variability of section-mean surface current due to westward propagating eddies can transiently lead to an uncertainty of one third or more of the measured transport. These observations show the impact of eddies and small-scale variability in disturbing the interpretation of *in situ* measurements and in the mass transport calculations, typically from estimates based on oceanographic cruises. Recent studies suggest that mesoscale activity not only influences the Coral Sea circulation by producing strong intraseasonal current fluctuations but may also be responsible for water mass mixing. Indeed, *Maes et al.* [2007] showed complex recirculation patterns within the Coral Sea: the trajectory of an Argo float reveals a possible connection from the NVJ to the NCJ. Similar trajectories of surface velocity drifters deployed in the North-Eastern part of the Coral Sea show the same phenomenon with a displacement from the NVJ to the NCJ [*Choukroun et al.*, 2010]. *Ganachaud et al.* [2008] also pointed out that the NCJ is possibly fed with waters that have circulated further north. Therefore, the joint

study of water mass properties and mesoscale features in the Coral Sea can provide a new insight into the potential role of eddies on the circulation, since coherent eddies are able to participate in the heat and salt exchanges between water masses [*Morrow et al.*, 2003; *Fieux et al.*, 2005].

In this study we propose to identify whether an active connection exists between the NCJ and the NVJ through water mass transport within eddies, and to quantify the part of the flow concerned by this connection on the long term. We use jointly *in situ* observations from an oceanographic cruise performed in the Coral Sea, Argo and satellite data to study the mesoscale structures associated with the water masses identified during the campaign. The snapshot picture revealed from the oceanographic cruise is extended with the analysis of Lagrangian particle trajectories at the scale of the Coral Sea calculated for up to two years. We analyse with Lagrangian particles the output of a numerical high-resolution simulation to follow the trajectory of water masses and their potential trapping by eddies. This approach is contributing to a better understanding of the circulation of Coral Sea water masses in a context of strong mesoscale variability.

2. Data and Methods

2.1. Observations

The Bifurcation cruise [*Maes*, 2012] was performed from 1 to 15 September 2012 under the auspices of the SPICE (SouthWest Pacific Oceanic Circulation and Climate Experiment) program which aims to observe, model, and better understand processes inducing the southwest Pacific oceanic circulation [*Ganachaud et al.*, 2014]. The *R/V Alis* transited from Nouméa (New Caledonia) to the Queensland Plateau (around 152-156°E and

16-19°S) before returning to Nouméa (Figure 1). The main objectives of the cruise were to study the sources and the characteristics of the NCJ [*Maes*, 2012].

Continuous measurements of horizontal currents have been performed by a *Shipboard-Acoustic Doppler Current Profiler* (S-ADCP RDI OS 75Hz). Instantaneous horizontal velocities are estimated between 24 and 488 m below the surface (every 16 m) with an error of $\pm$ 5cm s^{-1} [*Hummon and Firing*, 2003].

Temperature, salinity and dissolved oxygen have been collected with a Conductivity-Temperature-Depth (CTD) Seabird 911+ sensor to achieve 40 profiles from the surface down to 2000 m maximum. The locations of the 5 CTD profiles performed on 5 September 2012 and considered by this study are reported in Figure 1. They were planned to be located on the theoretical pathway of the NCJ. The CTD sensors have been pre- and post-calibrated and the resulting trend is linearly corrected, giving a classical precision of 0.001°C for temperature and 0.005 for salinity (according to the Practical Salinity scale, 1978). In the following temperature and salinity will refer to absolute salinity and conservative temperature respectively according to TEOS-10 standards [*McDougall et al.*, 2012]. Dissolved oxygen data (hereafter oxygen data) have been calibrated with Winkler-type discrete samples (with compliant residues according to international standards of -0.003 $\pm$ 1.730 μmol kg^{-1}) using post-cruise samples analyzed in laboratory [*Saout Grit et al.*, 2015].

Data from one Argo float (WMO id 5903381) are used as a complementary source of information. This specific float is very useful as it is the only one that sampled the studied area (Figure 1). The Argo profiler is equipped with CTD sensors and also an optode that provides oxygen profiles that are scarce in this region. The float was positioned in the

region of interest (around 13°S and 165°E) in January 2011. The Argo profiler data have been processed using a climatology-based quality control procedure [*Takeshita et al.*, 2013]. To compute the float trajectory at the parking depth near 1000 m, only the positions at the time of submergence and resurfacing are used [*Maes et al.*, 2007].

In situ measurements are systematically compared with two climatologies of the region: WOA2013 [*Locarnini et al.*, 2013; *Zweng et al.*, 2013] for temperature, salinity and oxygen and ISAS-13 atlas [*Gaillard et al.*, 2015] for temperature and salinity. *In situ* data are in good general agreement with climatologies considering that the maximum deviations are $\pm$ 0.02 in salinity, $\pm$ 0.05°C in temperature, but can reach up to $\pm$ 3°C at the surface, and $\pm$ 16 μmol kg^{-1} in oxygen.

Daily Ssalto/Duacs products [*Ducet et al.*, 2000], from AVISO (Archiving, Validation and Interpretation of Satellite Oceanographic 3) data base, for the period from 1 August 2012 to 31 October 2012, have been used to extract absolute geostrophic velocities in order to set the Bifurcation cruise in a larger context. Sea Level Anomalies (SLA) are calculated using several satellites (Cryosat-2, Jason-1/-2) and with respect to an average calculated over 1993-1998 to produce 1/4° $\times$ 1/4° daily maps on a Mercator grid (since 15 April 2014). There are many different methods to detect and track eddies [*Sadarjoen and Post*, 2000; *Doglioli et al.*, 2007; *Nencioli et al.*, 2010, among others]. Here we adopt some very simple definitions to investigate the origin and the dynamics of a specific eddy. The eddy detection and tracking have been done by visually inspecting consecutive daily maps of SSH. The eddy radius is defined with the outermost closed contour of sea surface height and the eddy center with the local extremum of sea surface height. The eddy average diameter is then calculated using the mean of the eddy

daily radii. In order to check the consistency of our eddy detection and tracking, we also performed a comparison with the published Chelton data set [*Chelton et al.*, 2011, http://cioss.coas.oregonstate.edu/eddies/].

2.2. Numerical Lagrangian diagnostics

The Lagrangian diagnostic tool Ariane was developed for tracing water mass movements, from the trajectories of numerical particles, in the output of ocean general circulation models [*Blanke and Raynaud*, 1997; *Blanke et al.*, 1999, http://www.univ-brest.fr/lpo/ariane]. This diagnosis allows to investigate all the possible fates and origins of water masses provided that a sufficiently high number of particles and of integration times are used. Here the particle trajectories are calculated in 2D space for two years with the same Lagrangian methodology as in *Maes and Blanke* [2015] for their tracking of plastic debris across the Coral Sea. Both current velocity datasets used here for the period 2010-2012 are provided by numerical models: i) the 1/12° PSY4V1R3 simulation by MERCATOR OCEAN provides the velocity fields at two separate levels, surface and 100 m depth, and ii) the Naval Research Laboratory (NRL) Layered Ocean Model (hereafter NLOM) by the International Pacific Research Center (Honolulu, Hawaii) provides a surface velocity field at 1/32°horizontal resolution.

Ariane is here used for integrating backward in time the trajectories of numerical particles initially distributed each day of 2012 across the section Ariane_SLI determined by its endpoints on Lihou Reef (at 152°E 17.4°S, see Figure 1) and the Great Barrier Reef (at 152°E 20.5°S). The calculations are stopped whenever the particles return to that initial section or are intercepted on the seven remote sections located around the Coral Sea (Figure 1). A small weight representative of the intensity of the local velocity is

associated with each numerical particle on its initial position. This weight (expressed as a mass transport) is assumed to be conserved along each trajectory. A mass transport is then calculated between any remote section and the Ariane_SLI section by summing the weights of all the particles that reached the remote section. This transport can be expressed as a percentage of the total transport and represents the intensity of the surface connection established between any remote section and the Ariane_SLI section. The rest of the analysis will focus on the connection between the Ariane_NVJ (see Figure 1) and Ariane_SLI sections. Following *Blanke et al.* [2006], the connection inferred from the horizontal movement of all the weighted particle, results as a 2D transport field. Thus, it can be expressed as a horizontal Lagrangian stream function that summarizes and shows the time average of the connection under study [*Blanke et al.*, 1999].

The analysis is restricted to some of the information provided by the horizontal movement of the particles. We compare the transport field inferred from the portions of trajectories associated with eddy-like variability and the transport field inferred from the full trajectory details. As in *Doglioli et al.* [2006], the details of individual trajectories are inspected to distinguish between portions captured by a rotating coherent eddy (either anticyclonic or cyclonic) and portions with no evidence of rotation. In this study the calculations are made from 6-hour positions sampled along the entire length of the trajectories. First, we compute the direction of the velocity vector at each position. Then, the change of direction (azimuth) of this vector is integrated along each trajectory. Finally, the azimuth difference over periods of N days (by considering the azimuth N/2 days after and N/2 days before any calculated position) lets us identify the portions of trajectories associated with eddy-like variability (when the difference is larger than a given threshold)

and portions of non-rotating behavior (when the difference is smaller than this threshold). The characteristic time it takes for a particle to circle twice around a coherent structure is determined from the mean diameter and tangential velocities at the edge of the eddy [*Hu et al.*, 2011; *Kersale et al.*, 2013]. Here, characteristic time scales of the order of 30 to 60 days were calculated using AVISO altimetry data for a particular anticyclonic eddy considered later in this study. A second calculation using S-ADCP velocities estimates the time scale to about 40 days. Thus, a threshold of N=40 days is considered to identify rotating portions of trajectory.

3. Results

3.1. Water mass analysis during the Bifurcation cruise

The Bifurcation dataset offers an interesting opportunity to study the properties of water masses reaching the western part of the Coral Sea compared to the water masses entering the Coral Sea from the east, completing the work of *Gasparin et al.* [2014]. During the cruise a total of 40 CTD profiles was performed. In the present study, we will focus on five CTD profiles (Figure 1). As the location of these CTDs is rather far from the entrance of the Coral Sea, the comparison with *Gasparin et al.* [2014] results can provide new information about pathways and exchanges during the journey of water masses across the Coral Sea. Figure 2 shows the five CTD profiles using the same color code as in Figure 1 (red for CTD 1 and 2 and blue for CTD 3, 4 and 5). The water column is thus separated into four distinct sections: surface waters ($\sim$ 0-100 m), upper thermocline waters ($\sim$ 100-350 m), lower thermocline waters ($\sim$ 350-600 m) and intermediate waters ($\sim$600-1000 m). Little differences can be observed between the CTD 1 and 2 profiles and the CTD 3, 4 and

241 5 profiles. The analysis of the remaining CTD profiles (data not shown) shows patterns
242 similar to CTD 3, 4 and 5 profiles (corresponding to blue crosses in Figure 1).

243 Figure 3a shows the Temperature-Salinity (T-S) diagram of the water column down to
244 2000 m for the five CTD profiles. The tight distribution of the profiles is overall consistent
245 with *Tomczak and Godfrey* [2013] results based on CTD measurements in the eastern Coral
246 Sea, but also with two climatologies: WOA2013 and ISAS-13. As a guideline, the water
247 mass properties defined by *Gasparin et al.* [2014] are indicated in our T-S diagrams. At
248 the levels of surface waters (TSW) and upper thermocline waters (SPTWS and SPTWN)
249 our profiles follow the general layout expected in this area (salinity maximum at the 22°C
250 isotherm) for a water sigma-t around 25 kg m^{-3}. At the level of the salinity maximum,
251 the salinity is fresher than for the waters entering the Coral Sea, which implies a loss of
252 salt across the Coral Sea. The overlapping of the profiles in this layer back up the fact
253 that water masses are probably mixed with each other. In the lower thermocline, CTD
254 profiles show properties close to that of PEW and WSPCW. The same applies for the
255 intermediate waters (AAIW). Moreover, a zoom on the lower thermocline reveals a strong
256 PEW signature for the waters sampled during the cruise (Figure 3b). This observation
257 is unexpected considering that *Gasparin et al.* [2014] put at ∼70% the contribution of
258 WSPCW in the western part of the Coral Sea, compared to ∼20-30% for PEW. This result
259 suggests a stronger influence of PEW in this area than previously expected. Nevertheless,
260 at this stage, the T-S diagram is not sufficient to assess with absolute certainty the origins
261 of water masses sampled during the Bifurcation cruise.

262 *Rochford* [1968], *Tomczak and Hao* [1989] and *Maes et al.* [2007], among others, sug-
263 gested the use of oxygen concentration for a better discrimination of the water masses in

this region. Figures 4 (a) and (b) show respectively the Salinity-Oxygen (S-O_2) and the Temperature-Oxygen (T-O_2) diagrams from CTD data. The use of oxygen data allows us now to clearly separate the profiles vertically into two distinct parts. The upper part, identified with small markers, is composed of similar surface waters for all profiles and by upper thermocline waters showing an oxygen minimum for CTD 3, 4 and 5 ($\sim$135 μmol kg^{-1}, in blue) and a maximum for CTD 1 and 2 ($\sim$170 μmol kg^{-1}, in red). The upper part of the S-O_2 and T-O_2 diagrams will be discussed in Section 4. The lower part, identified with big markers, is composed of distinct lower thermocline waters ($\sim$350-600 m) for the red and blue profiles and by similar intermediate waters at the AAIW level. Clear differences exist between the profiles in the lower thermocline. At this level, the CTD 3, 4 and 5 profiles show an increase in oxygen concentration up to an oxygen maximum ($\sim$190 μmol kg^{-1}) reached just before the AAIW level, consistent with WSPCW waters. The CTD 1 and 2 profiles show a reverse pattern characterized by an oxygen minimum ($\sim$145 μmol kg^{-1}) at 35 and 13° C. This oxygen minimum is likely to be the oxygen minimum characterising the PEW. In comparison with *Tomczak and Hao* [1989] results, we can assume that CTD 1 and 2 reveal the signature of PEW, and consequently of NVJ-like water masses, whereas CTD 3, 4 and 5 are rather similar to WSPCW transported by the NCJ.

Data from an Argo float (WMO id 5903381) that sampled both the NVJ and NCJ are superimposed on the S-O_2 and T-O_2 diagrams issued from the CTD collected during the cruise (Figure 5). Two groups of profiles are distinguished as they are considered to be fairly typical of NVJ and NCJ waters (Figure 1). In general, the Argo profiles show the same vertical distribution with an offset towards lower oxygen concentrations for the NVJ

waters, especially for waters below the lower thermocline. At this depth, the differences in oxygen concentrations between NVJ and NCJ waters almost reach 20 μmol kg^{-1}. The distribution of the Argo profiles is fairly identical to the PEW and WSPCW profiles shown by *Tomczak and Hao* [1989]. This comparison allows us to deduce with confidence that green (purple) profiles are typical of NVJ (NCJ) waters. The difference in oxygen concentration between the CTD 1 and 2 and CTD 3, 4 and 5 profiles is in the same range compared to the difference between NVJ and NCJ oxygen properties. Indeed in the lower thermocline, the CTD 3, 4 and 5 profiles are rather similar to the NCJ profiles whereas the CTD 1 and 2 profiles show an oxygen minimum similar to that of the NVJ waters. The comparison between CTD profiles and Argo profiles suggests different sources for the waters sampled during the Bifurcation cruise: CTD 1 and 2 profiles are rather typical of NVJ waters whereas CTD 3, 4 and 5 profiles suggest a NCJ origin.

As the Bifurcation area is located on the theoretical pathway of NCJ waters, we assume here that a dynamic process is able to bring in water masses with a NVJ-like signature. To explore this hypothesis, we investigate the regional circulation during the Bifurcation cruise and in particular the mesoscale activity of the Coral Sea.

3.2. The mesoscale context during summer 2012

The comparison of the measured currents and daily surface velocity fields derived from AVISO altimetry shows equivalent coherent structures along the Bifurcation route. Our analysis leads to the identification of 9 eddies, crossing the route of the cruise and detected either with AVISO at the surface or with S_ADCP measurements along the first top 0-500 m of the water column (Figures S1-2, Supporting Information). These structures may have an influence on water mass exchanges or transports at short time scale. An

example of a daily image of surface currents is shown in Figure 1. As expected from earlier observations, the Coral Sea is subject to intense mesoscale activity indicated by the presence of numerous eddies. A westward flow is detectable north of the Coral Sea, but the main jets are not identifiable as a consequence of strong mesoscale activity. The consistency between the *in situ* measurements and the structures detected by altimetry allows to use AVISO data over the previous and following month to assess the eddies' history. The spatial and temporal coverage of satellite-derived surface currents allows the tracking of the structures and to study their properties. Most of the structures are cyclonic (6 out of 9), but the largest ones are anticyclonic with a diameter between 150 and 400 km. Despite some differences, all the structures propagate westward at about 6 km day^{-1}.

The relative vorticity calculated with the AVISO absolute geostrophic current is shown in Figure 6. This parameter allows to identify eddies but also to investigate their surface extension and the shape of their theoretical core delineated by the region inside the contour of zero relative vorticity [*Korotaev and Fedotov*, 1994; *Early et al.*, 2011]. The map in Figure 6 reveals the presence of two intense eddies: a cyclonic eddy (hereafter C) at 16° S and 152.5° E and an anticyclonic eddy (hereafter A). In the following, we focus only on eddy A as the water mass analysis of the CTD casts located on the route crossed by eddy C on 5 September 2012 did not reveal any influence of this eddy on water mass exchange or transport (data not shown). The southern branch of eddy A, detected either with AVISO or ADCP currents, crosses the CTD transect at the same time as the CTD 1, 2, 3, 4 and 5 samplings. Consequently the differences highlighted with the water mass analysis in CTD 1 and 2 profiles seem to be linked to the passage of eddy A. The time-

tracking analysis using AVISO reveals that eddy A left the north-eastern region in August, propagated for two months south-westwardly, arriving north of Lihou Reef early October (Figure 7). Its position and trajectory crossing both theoretical pathways of the NVJ and the NCJ, could explain the presence of NVJ-like water masses at 17°S during the Bifurcation cruise. Following the theory of *Early et al.* [2011] we suggest that eddy A has trapped NVJ water masses during its formation in the north-eastern Coral Sea and has transported them into the pathway of NCJ waters. Moreover the eddy trajectory crossing meridionally both jets is a key aspect of the water mass transport. Within the Chelton data set we found 7 anticyclonic eddies similar to eddy A that travelled from the NVJ to the NCJ over the period October 1992 through April 2012 confirming that such trajectories and exchanges between the NVJ and the NCJ through eddy displacements are not a one shot observation.

The mesoscale context allows to identify a dynamic process that could explain the presence of NVJ-like water masses in the Bifurcation area: the transport of NVJ waters and properties by mesoscale eddies. In order to test the persistence of such a connection between the NVJ and the NCJ we have chosen to analyse with a Lagrangian perspective the long-term outputs from two ocean general circulation models.

3.3. Evidence of a connecting pathway across the Coral Sea

The Lagrangian toolkit Ariane provides the trajectories of the particles crossing the Ariane_SLI section. This analysis is used to determine the origins of water masses that reach this area of the Coral Sea. We first check that both velocity data sets, used to run this analysis and associated, respectively, with MERCATOR and NLOM (see Section 2.2), reflect properly the mesoscale variability sampled by the AVISO gridded product, and

especially eddy A. The barotropic circulation identified with S_ADCP currents suggests that the circulation is similar at the surface and deeper. Moreover as both velocity data sets gave similar results in terms of connection, in the following, we focus on the analysis of the results obtained with the higher resolution NLOM model.

Our Lagrangian analysis shows that the particles reaching the Ariane_SLI section can originate from all the sections that bound the domain of integration of the trajectories, but with a predominant recirculation across the Ariane_SLI section (34% of the transport, not shown). The remaining 66% of the incoming transport is composed of particles whose origins are distributed across the interception sections located further north or southeast. We estimate that 3% of the surface flow across the Ariane_SLI section originates from the Ariane_NVJ section (Figure 8) and 4% from the Ariane_NCJ section. This double origin from both sides of Vanuatu is interesting because, until now, the westward flow crossing the Ariane_SLI section was thought to be entirely made of locally recirculating waters and NCJ waters flowing south of Vanuatu [*Tomczak and Godfrey*, 2013]. This Lagrangian description suggests that the western part of the NCJ is also fed with PEW and SPTWN. The mean surface connection time between the Ariane_NVJ and Ariane_SLI sections is about 8 months, but we also identify faster connection times, even as short as 2 months. This numerical estimation is consistent with the results obtained with AVISO altimetry. Indeed, eddy A travels for a month across the Coral Sea, from 163°E until it reaches the Bifurcation area at 155°E, and needs approximately one more month to reach the Australian Coast. Moreover, the stream function between Ariane_SLI and Ariane_NVJ sections (Figure 9) show a new south-westward pathway for the particles originating from the Ariane_NVJ section. The spreading of the contours of this stream function between

155°E and 166°E and between 13°S and 17°S indicates that almost the entire Coral Sea is affected by this connection.

Each trajectory, that is part of the connection, is inspected in detail to check the potential trapping and transport of waters by coherent structures. The portions of trajectories associated with eddy-like variability, as defined from the quantification of successive azimuth differences (cf. Section 2.2), reveal the strong influence of mesoscale activity in trapping particles all over the Coral Sea (see Figure S3, Supporting Information). They also allow evaluating the contribution of eddies in the connection made from the Ariane_NVJ and Ariane_SLI sections. This contribution is expressed in Figure 8 as a percentage by means of colored diamonds whose size is proportional to the local intensity of the transfer (a piece of information that tallies with the spacing of the contours). The connection is intensified at 17°S between 150°E and 160°E on the western part of the NCJ theoretical pathway, and at the entrance of the NVJ in the Coral Sea (at 13°S between 160°E and 165°E). This result is consistent with the positions usually accepted for the two jets. In between them, the connection is less intense but eddies can contribute up to 50% of the transfer. On average over the domain, the proportion of the transfer associated with eddy-like trapping can be estimated between 10% and 20%.

Finally, the Lagrangian framework we just introduced can be used to isolate the proportion of anticyclonic eddies involved in the fraction of the transfer associated with eddy-like trapping (Figure 9). The contribution from anticyclonic eddies varies between 10% and 90% in the intermediate area between the two jets. It amounts to 70% all the way to 90% between 15° S and 17° S, and, 155° E and 160° E. This area turns out to match the location of eddy A that locally connects NVJ and NCJ water masses during the Bifurca-

tion cruise. By comparison, the areas where anticyclonic eddies have the least influence are located in the theoretical pathway of the jets (especially at the NVJ entrance in the Coral Sea and in the southern part of the NCJ). This matches the observations during the Bifurcation cruise and suggests the role of anticyclonic eddies in connecting both jets by transporting water masses meridionally while their main pathways are zonal.

4. Discussion

The analysis of the lower thermocline waters evidenced the signature of PEW-like waters on the CTD 1 and 2 profiles, thus with an origin from the NVJ. Instead, the agreement of the CTD 3, 4 and 5 profiles with the properties of the WSPCW suggests a NCJ origin. In the upper thermocline (see Figure 4) an oxygen minimum at 18°C and 35.6 for CTD 3, 4 and 5 suggests that the CTD 1 and 2 profiles are more oxygenated than the CTD 3, 4 and 5. In the light of our previous assumption associating CTD 1 and 2 with the NVJ and CTD 3, 4 and 5 with the NCJ, this result is in contradiction with the observations of *Tomczak and Godfrey* [2013] and *Gasparin et al.* [2014]. Indeed, these two studies showed that both NVJ upper (SPTWN) and lower (PEW) thermocline waters are continuously less oxygenated than NCJ upper (SPTWS) and lower (WSPCW) thermocline waters in the vertical. Following this, the upper thermocline waters sampled during CTD 3, 4 and 5, showing an oxygen minimum cannot be associated with oxygenated NCJ waters. This oxygen minimum may originate from a mixture with Pacific equatorial waters whose oxygen properties agree with this minimum. Mixing processes are indeed supported by the complex overlapping of the profiles evidenced at the level of the upper thermocline waters in Figure 3. In addition to mixing processes, the oxygen minimum may be accentuated by biological mechanisms that are not considered in this study. The complex interplay

of physical and biological processes that possibly affect water mass modifications gives us less confidence in the analysis of the upper part of the water column than in the one of the lower part which is more conservative.

Lower thermocline waters of CTD 1 and 2, located at 17-18° S, are identified as a mixed form of PEW. This observation remains unexpected because *Tomczak and Godfrey* [2013] have previously identified a 'Water Mass Boundary' (WMB) at 15°S separating the pathway of the PEW in the northern part and the pathway of the WSPCW in the southern part of the Coral Sea. It suggests that the geographical extension of the PEW should be reconsider with care and more observations. Moreover in this study we have suggested a mechanism of water masses transport through eddy trapping and displacement to explain this observation. This assumption relies on the definition of *Early et al.* [2011] who demonstrated that a theoretical circular eddy is able to transport within its core the waters trapped during the eddy formation. However in our case of study we found in eddy A, the signature of NVJ waters mixed with waters encountered along its track [*Kaneko et al.*, 2015]. The position of the CTD 1 and 2, almost on the edge of this eddy as well as the irregular shape of the latter may explain the differences between the characteristics of PEW waters at the entrance of the Coral Sea [*Gasparin et al.*, 2014] and those sampled during the cruise. However, the signature of PEW is high enough to identify the NVJ-NCJ connection due to water mass transport through eddy displacement. This direct *in situ* observation remains one of a kind. *Lumpkin* [2016]'s recent study, using surface drifter trajectories, identified two eddies (an anticyclone and a cyclone) travelling from the NVJ to the NCJ, which reinforce our results and highlight the important role of eddies in conditioning the water mass circulation in the Coral Sea.

The origin and the mechanism of transport of the water masses sampled during the Bifurcation cruise have been confirmed by our Lagrangian analysis applied to a model velocity field. Indeed, it demonstrates meridional exchanges between the NVJ and the NCJ, as already noted by *Maes et al.* [2007] and *Qiu et al.* [2009]. Our Lagrangian study estimates the contribution of anticyclonic eddies to this transfer, in the light of the one-time connection identified during the Bifurcation cruise through the southward displacement of anticyclonic eddy A. This is not a classical behavior for anticyclonic eddies that are mostly advected equatorward. However at global scale *Chelton et al.* [2007] estimated that 31% of anticyclonic eddies propagating westward have a poleward deflection similar as eddy A. This percentage is large enough to support the connection highlighted here through the circulation of anticyclonic eddies between the NVJ and the NCJ. Moreover the contribution of anticyclonic eddies is found to be the highest in the band 155° E-160° E around 16° S. This zone corresponds to the area identified by *Qiu et al.* [2009, see Fig. 1b] as a region of relatively high eddy variability. They studied the eastward Coral Sea Countercurrent (CSCC) in this band along 16° S, driven by the dipolar wind stress curl forcing localized in the lee of Vanuatu. They also suggested that the barotropic instability of the horizontally-sheared NCJ-CSCC-NVJ system is responsible for eddy variability in the CSCC band. Thus, the connection between the NVJ and the NCJ through eddy circulation in this area could also be a consequence of the high eddy kinetic energy (EKE) generated by barotropic instabilities in the Coral Sea. In addition, our Lagrangian analysis confirms the intense recirculation zones identified by *Kessler and Cravatte* [2013a]; *Ganachaud et al.* [2014] on the edge of the Australian continent and south of the Solomon Sea. Interestingly they also indicate strong recirculation from

the north and the south of the Coral Sea. These features coupled with important mixing processes need to be studied in detail to fully understand the different water mass pathways across the Coral Sea.

In this study the role of mesoscale activity on the transport of water masses is well-demonstrated but it can also be estimated by calculating the transport from *in situ* measurements. The transports calculated with S_ADCP and associated with each transect of the cruise are given in Figure S4 (Supporting Information). Transects 1 and 8 are out of the NCJ pathway but give an interesting example of the eddy-induced strong temporal variability. Indeed, transects 1 and 8 show a difference of about 15 Sv while they follow the same path with a time interval between them of only 15 days. This difference, due to eddy displacements across the transects of the cruise, can reach the order of magnitude of the transport of the jets. This observation underlines the role of mesoscale activity in introducing large temporal variability completing the study of *Kessler and Cravatte* [2013b] but also reinforces the question about the role of eddies on water mass transport.

5. Conclusions

The Bifurcation cruise dataset offered an opportunity to assess mesoscale activity in the Coral Sea through current measurements and water mass sampling. The analysis of water masses, sampled either by CTD casts or Argo float, together with the study of mesoscale activity from satellite-derived velocity, allows to identify an anticyclonic eddy that participates in the transport of NVJ-like waters in the pathway of NCJ waters. Indeed, ocean eddies can transfer heat, salinity, oxygen and other tracers and thus play an important role on water mass composition and mixing [*Eady*, 1957; *Morrow et al.*, 2003]. The Lagrangian analysis using velocity data from the NLOM model also shows complex trajectories in the

Coral Sea. Our analysis highlights the challenges of determining water mass origins and pathways in the Coral Sea due to intense mixing partially caused by mesoscale activity. Both *in situ* and numerical observations indicate a dynamic connection between the two main jets of the Coral Sea, the NVJ and the NCJ, through eddy circulation. Our Lagrangian analysis suggests that anticyclonic eddy circulation is a major component of this connectivity. This *indirect* pathway for NVJ waters, through mesoscale activity, offers a new alternative to both *direct* pathways of NVJ waters towards the Australian Coast at 13°S and towards the Solomon Sea [*Ganachaud et al.*, 2014]. This study thus provides a new vision of the dynamics of the Coral Sea considering mesoscale activity as a key component in the structuring of the regional water mass circulation. Future work on the Coral Sea must take into account the active role of eddies to better understand the pathways and transformations of the waters of the south-west Pacific. Work is underway to apply this kind of analysis in the context of the OUTPACE cruise [*Moutin and Bonnet*, 2015] in order to study the dynamics of the entire south-west Pacific.

Acknowledgments.

Special thanks to the officers and crew of the R/V Alis who operated the Bifurcation cruise. The cruise data have been archived by the SISMER data center (www.ifremer.fr/sismer/). The Bifurcation project also received the support of the SPICE program, led by Dr Alexandre Ganachaud (IRD). The Argo data are collected and made freely available by the International Argo Project and the national programs that contribute to it (www.argo.ucsd.edu, argo.jcommops.org). The altimeter products were produced by Ssalto/Duacs and distributed by Aviso, with support from CNES (http://www.aviso.altimetry.fr/duacs/). The current velocity data were provided by

513 MERCATOR OCEAN. Special thanks go to Dr Virginie Thierry and Dr Thomas Bouinot
514 for the calibration of the oxygen data collected with the Argo floats, to Dr Fabienne Gail-
515 lard for ISAS analysis and to Dr Gérard Eldin and Dr Frédéric Marin for their expertise on
516 the S_ADCP data. The authors are grateful for the support of the OUTPACE project (PIs
517 T. Moutin and S. Bonnet) and CNES (contract number ZBC 4500048836). L. Rousselet
518 is financed by a MRT Ph.D grant. Finally, we thank the reviewers for their constructive
519 and detailed comments.

References

Blanke, B., and S. Raynaud (1997), Kinematics of the Pacific Equatorial Undercurrent: an Eulerian and Lagrangian approach from GCM results, *J. Phys. Oceanogr.*, *27*(6), 1038–1053.

Blanke, B., M. Arhan, G. Madec, and S. Roche (1999), Warm water paths in the equatorial Atlantic as diagnosed with a general circulation model, *J. Phys. Oceanogr.*, *29*(11), 2753–2768.

Blanke, B., M. Arhan, and S. Speich (2006), Salinity changes along the upper limb of the Atlantic thermohaline circulation, *Geophys. Res. Lett.*, *33*(6).

Burrage, D., S. Cravatte, P. Dutrieux, A. Ganachaud, R. Hughes, W. Kessler, A. Melet, C. Steinberg, and A. Schiller (2012), Naming a western boundary current from Australia to the Solomon Sea, *CLIVAR Exchanges*, *17*(58; 1).

Chelton, D. B., M. G. Schlax, R. M. Samelson, and R. A. de Szoeke (2007), Global observations of large oceanic eddies, *Geophys. Res. Lett.*, *34*(15).

Chelton, D. B., M. G. Schlax, and R. M. Samelson (2011), Global observations of nonlinear mesoscale eddies, *Prog. Oceanogr.*, *91*(2), 167–216.

Choukroun, S., P. V. Ridd, R. Brinkman, and L. I. McKinna (2010), On the surface circulation in the western Coral Sea and residence times in the Great Barrier Reef, *J. Geophys. Res-O.*, *115*(C6).

Couvelard, X., P. Marchesiello, L. Gourdeau, and J. Lefèvre (2008), Barotropic zonal jets induced by islands in the southwest Pacific, *J. Phys. Oceanogr.*, *38*(10), 2185–2204.

Doglioli, A., M. Veneziani, B. Blanke, S. Speich, and A. Griffa (2006), A Lagrangian analysis of the Indian-Atlantic interocean exchange in a regional model, *Geophys. Res. Lett.*,

542 *33*(14).

543 Doglioli, A., B. Blanke, S. Speich, and G. Lapeyre (2007), Tracking coherent structures
544 in a regional ocean model with wavelet analysis: Application to Cape Basin eddies,
545 *J. Geophys. Res-O.*, *112*(C5).

546 Ducet, N., P.-Y. Le Traon, and G. Reverdin (2000), Global high-resolution mapping
547 of ocean circulation from TOPEX/Poseidon and ERS-1 and-2, *J. Geophys. Res-O.*,
548 *105*(C8), 19,477–19,498.

549 Eady, E. (1957), The general circulation of the atmosphere and oceans.

550 Early, J. J., R. Samelson, and D. B. Chelton (2011), The evolution and propagation of
551 quasigeostrophic ocean Eddies*, *J. Phys. Oceanogr.*, *41*(8), 1535–1555.

552 Emery, W. (2001), Water types and water masses, *Enc. Ocean Sci.*, *6*, 3179–3187.

553 Fieux, M., R. Molcard, and R. Morrow (2005), Water properties and transport of the
554 Leeuwin Current and eddies off Western Australia, *Deep-Sea Res. I*, *52*(9), 1617–1635.

555 Gaillard, F., T. Reynaud, V. Thierry, N. Kolodziejczyk, and K. von Schuckmann (2015),
556 In-situ based reanalysis of the global ocean temperature and salinity with ISAS: vari-
557 ability of the heat content and steric height, *J. Clim.*, doi:10.1175/JCLI-D-15-0028.1.

558 Ganachaud, A., L. Gourdeau, and W. Kessler (2008), Bifurcation of the Subtropical South
559 Equatorial Current against New Caledonia in December 2004 from a Hydrographic
560 Inverse Box Model*, *J. Phys. Oceanogr.*, *38*(9), 2072–2084.

561 Ganachaud, A., S. Cravatte, A. Melet, A. Schiller, N. Holbrook, B. Sloyan, M. Widlansky,
562 M. Bowen, J. Verron, P. Wiles, et al. (2014), The Southwest Pacific Ocean circulation
563 and climate experiment (SPICE), *J. Geophys. Res-O.*, *119*(11), 7660–7686.

564 Gasparin, F. (2012), Caractéristiques des Masses d'Eau, Transport de Masse et Variabilité
565 de la Circulation Océanique en mer de Corail (Pacifique sud-ouest), Ph.D. thesis, Uni-
566 versité Toulouse III - Paul Sabatier, Sciences de l'Univers, de l'Environnement et de
567 l'Espace (SDU2E).

568 Gasparin, F., C. Maes, J. Sudre, V. Garcon, and A. Ganachaud (2014), Water mass analy-
569 sis of the Coral Sea through an Optimum Multiparameter method, *J. Geophys. Res-O.*,
570 *119*(10), 7229–7244.

571 Gourdeau, L., W. Kessler, R. Davis, J. Sherman, C. Maes, and E. Kestenare (2008), Zonal
572 jets entering the Coral Sea, *J. Phys. Oceanogr.*, *38(3)*(715725).

573 Hristova, H. G., W. S. Kessler, J. C. McWilliams, and M. J. Molemaker (2014), Mesoscale
574 variability and its seasonality in the Solomon and Coral Seas, *J. Geophys. Res-O.*,
575 *119*(7), 4669–4687.

576 Hu, Z., A. Petrenko, A. Doglioli, and I. Dekeyser (2011), Study of a mesoscale anticyclonic
577 eddy in the western part of the Gulf of Lion, *J. Mar. Sys.*, *88*(1), 3–11.

578 Hummon, J., and E. Firing (2003), A Direct Comparison of Two RDI Shipboard ADCPs:
579 A 75-kHz Ocean Surveyor and a 150-kHz Narrow Band, *J. Atmos. Ocean. Technol.*,
580 (872-888).

581 Kaneko, H., S. Itoh, S. Kouketsu, T. Okunishi, S. Hosoda, and T. Suga (2015), Evolution
582 and modulation of a poleward-propagating anticyclonic eddy along the Japan and Kuril-
583 Kamchatka trenches, *J. Geophys. Res-O.*, *120*, 4418–4440.

584 Kersale, M., A. Petrenko, A. Doglioli, I. Dekeyser, and F. Nencioli (2013), Physical char-
585 acteristics and dynamics of the coastal Latex09 Eddy derived from in situ data and
586 numerical modeling, *J. Geophys. Res-O.*, *118*(1), 399–409.

587 Kessler, W., and S. Cravatte (2013a), Mean circulation of Coral Sea, *J. Geophys. Res-O.*,
588 *118*, 1–26, doi:10.1002/2013JC009117.

589 Kessler, W. S., and S. Cravatte (2013b), ENSO and short-term variability of the South
590 Equatorial Current entering the Coral Sea, *J. Phys. Oceanogr.*, *43*(5), 956–969.

591 Kessler, W. S., and L. Gourdeau (2007), The Annual Cycle of Circulation of the Southwest
592 Subtropical Pacific, Analyzed in an Ocean GCM*, *J. Phys. Oceanogr.*, *37*(6), 1610–
593 1627.

594 Korotaev, G. K., and A. B. Fedotov (1994), Dynamics of an isolated barotropic eddy on
595 a beta-plane, *J. Fluid Mech.*, *264*, 277–301.

596 Locarnini, R. A., A. V. Mishonov, J. I. Antonov, T. P. Boyer, H. E. Garcia, O. K.
597 Baranova, M. M. Zweng, C. R. Paver, J. R. Reagan, D. R. Johnson, M. Hamilton, and
598 D. Seidov (2013), *World Ocean Atlas 2013, Volume 1: Temperature*, S. Levitus, Ed.,
599 A. Mishonov Technical Ed.; NOAA Atlas NESDIS 73, 40 pp.

600 Lumpkin, R. (2016), Global characteristics of coherent vortices from surface drifter tra-
601 jectories, *J. Geophys. Res-O.*, *121*, doi:10.1002/2015JC011435.

602 Maes, C. (2012), BIFURCATION cruise, Alis R/V, doi:10.17600/12100100.

603 Maes, C., and B. Blanke (2015), Tracking the origins of plastic debris across the Coral
604 Sea: A case study from the Ouvéa Island, New Caledonia, *Mar. Pollut. Bull.*, *97*(1),
605 160–168.

606 Maes, C., L. Gourdeau, X. Couvelard, and A. Ganachaud (2007), What are the origins
607 of the Antarctic Intermediate Waters transported by the North Caledonian Jet?, *Geo-*
608 *phys. Res. Lett.*, *34*(21).

McDougall, T., D. Jackett, F. Millero, R. Pawlowicz, and P. Barker (2012), A global algorithm for estimating absolute salinity, *Ocean Sci.*, *8*(6), 1123–1134.

Morrow, R., F. Fang, M. Fieux, and R. Molcard (2003), Anatomy of three warm-core Leeuwin Current eddies, *Deep-Sea Res. II*, *50*(12), 2229–2243.

Moutin, T., and S. Bonnet (2015), OUTPACE cruise, RV L'Atalante, doi:10.17600/15000900.

Nencioli, F., C. Dong, T. Dickey, L. Washburn, and J. C. McWilliams (2010), A vector geometry-based eddy detection algorithm and its application to a high-resolution numerical model product and high-frequency radar surface velocities in the Southern California Bight, *J. Atmos. Ocean. Technol.*, *27*(3), 564–579.

Qiu, B., S. Chen, and W. S. Kessler (2009), Source of the 70-Day Mesoscale Eddy Variability in the Coral Sea and the North Fiji Basin*, *J. Phys. Oceanogr.*, *39*(2), 404–420.

Ridgway, K., and J. Dunn (2003), Mesoscale structure of the mean East Australian Current System and its relationship with topography, *Prog. Oceanogr.*, *56*(2), 189–222.

Rochford, D. (1968), The continuity of water masses along the western boundary of the Tasman and Coral Seas, *Mar. Fresh. Res.*, *19*(2), 77–90.

Rogé, M., R. A. Morrow, and G. Dencausse (2015), Altimetric Lagrangian advection to reconstruct Pacific Ocean fine-scale surface tracer fields, *Ocean Dynam.*, *65*(9-10), 1249–1268.

Sadarjoen, I. A., and F. H. Post (2000), Detection, quantification, and tracking of vortices using streamline geometry, *Comput. Graph.*, *24*(3), 333–341.

Saout Grit, C., A. Ganachaud, C. Maes, L. Finot, L. Jamet, F. Baurand, and J. Grelet (2015), Calibration of CTD oxygen data collected in the Coral Sea during the 2012

632 BIFURCATION Cruise, *Mercator Ocean-Quaterly Newsletter*, (52), 34–38.

633 Sokolov, S., and S. Rintoul (2000), Circulation and water masses of the southwest Pacific:
634 WOCE section P11, Papua New Guinea to Tasmania, *J. Mar. Res.*, *58*(2), 223–268.

635 Takeshita, Y., T. R. Martz, K. S. Johnson, J. N. Plant, D. Gilbert, S. C. Riser, C. Neill,
636 and B. Tilbrook (2013), A climatology-based quality control procedure for profiling float
637 oxygen data, *J. Geophys. Res-O.*, *118*(10), 5640–5650.

638 Thompson, R., and G. Veronis (1980), Transport calculations in the Tasman and Coral
639 seas, *Deep-Sea Res. I*, *27*(5), 303–323.

640 Tomczak, M., and J. S. Godfrey (2013), *Regional oceanography: an introduction*, Elsevier.

641 Tomczak, M., and D. Hao (1989), Water masses in the thermocline of the Coral Sea,
642 *Deep-Sea Res. I*, *36*(10), 1503–1514.

643 Webb, D. (2000), Evidence for shallow zonal jets in the South Equatorial Current region
644 of the southwest Pacific, *J. Phys. Oceanogr.*, *30(4)*(706720).

645 Wyrtki, K. (1962), The Subsurface Water Masses in the Western South Pacific Ocean,
646 *Aust J Mar Fresh Res.*, *13(1)*, 18–47.

647 Zweng, M., J. Reagan, J.R.and Antonov, R. Locarnini, A. Mishonov, T. Boyer, H. Garcia,
648 O. Baranova, D. Johnson, D. Seidov, and M. Biddle (2013), *World Ocean Atlas 2013,*
649 *Volume 2: Salinity*, S. Levitus, Ed., A. Mishonov Technical Ed.; NOAA Atlas NESDIS
650 74, 39 pp.

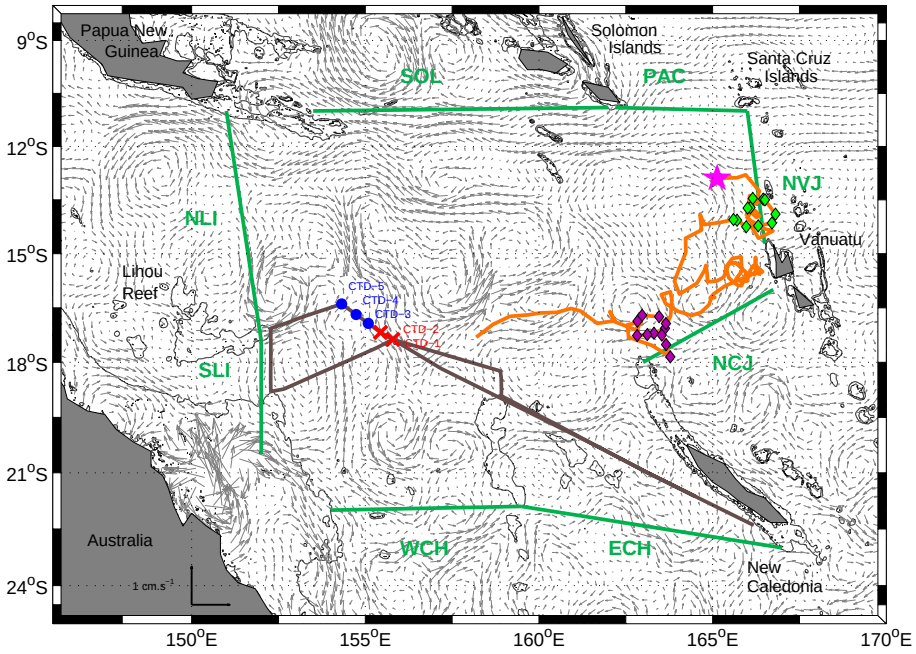

Figure 1. Daily absolute surface geostrophic currents [m s^{-1}] of the Coral Sea derived from the AVISO dataset (5 Sept. 2012). The Bifurcation cruise route is indicated with a brown line. The positions of the CTD stations are indicated with red crosses (southern part of the CTD transect, CTD 1 and 2) and blue points (northern part of the CTD transect, CTD 3, 4 and 5). The deployment position and the trajectory of the Argo float WMO Id 5903381 are indicated by the pink star and the orange line, respectively. Two sets of Argo profiles are identified as belonging to the NVJ waters pathway (green diamonds) and to the NCJ waters pathway (purple diamonds). The green lines show the sections used for the Ariane Lagrangian analysis. These sections are, clockwise: SLI ('South Lihou'), from Lihou Reef to the Great Coral Barrier; NLI ('North Lihou'), from Lihou Reef to Papua New Guinea; SOL ('Solomon Sea'), from Papua New Guinea to the Solomon Islands; PAC ('Pacific'), from the Solomon Islands to the Santa Cruz Islands; NVJ ('North Vanuatu Jet'), from the Santa Cruz Islands to the Vanuatu Archipelago; NCJ ('North Caledonian Jet'), from the Vanuatu Archipelago to the northernmost extension of New Caledonia coral reef; ECH ('East Chesterfield'), from New Caledonia to the Chesterfield Archipelago; WCH ('West Chesterfield'), from the Chesterfield Archipelago to the Great Coral Reef. Isobaths 500 and 1000 m are also represented by black lines.

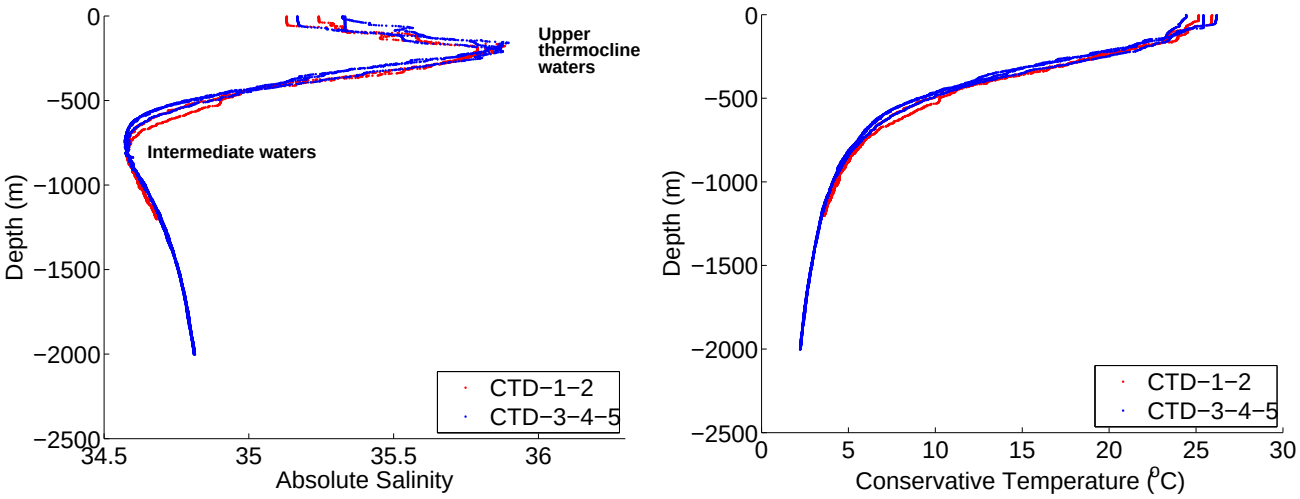

Figure 2. Vertical profiles of absolute salinity (left) and conservative temperature (right) for the CTD profiles on the CTD transect of the Bifurcation cruise identified in red and in blue in Figure 1. Upper thermocline and intermediate waters are indicated corresponding to the salinity minimum and maximum respectively.

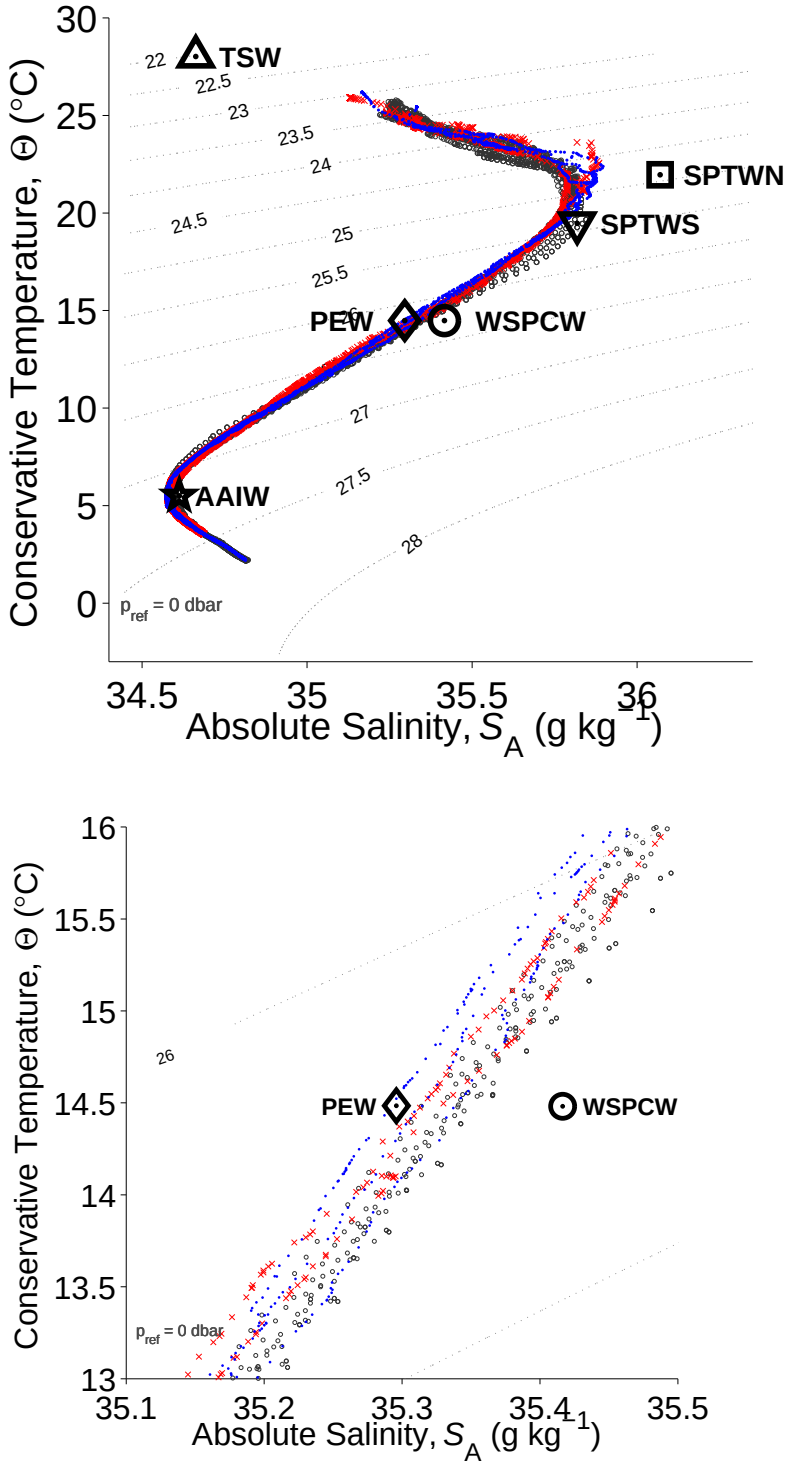

Figure 3. (a) Conservative temperature-Absolute salinity diagram for the CTD profiles on the CTD transect of the Bifurcation cruise identified in red and in blue in Figure 1. ISAS-13 profiles from the Argo Atlas are also shown with grey circles, and the properties of the main water masses identified by *Gasparin et al.* [2014] at the entrance of the Coral Sea with bold black symbols. (b) Same as (a) but zoomed on the lower thermocline.

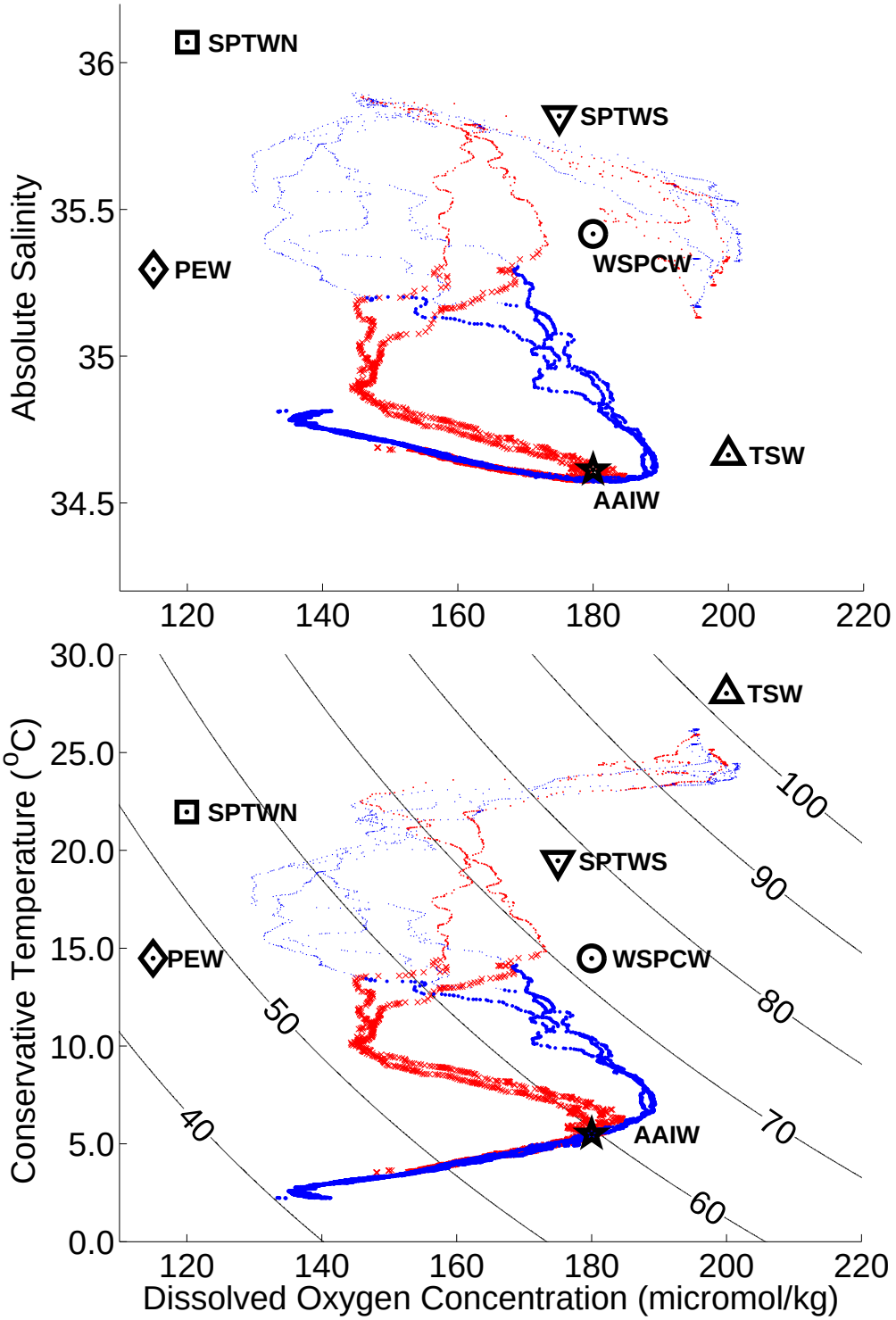

Figure 4. (a) Absolute salinity-Dissolved oxygen diagram for the CTD profiles identified in Figure 1. (b) Conservative temperature-Dissolved oxygen diagram for the same CTD stations as (a). The upper part of the diagram is identified with small markers (layer 0-350 m) and the lower part is identified with big markers (layer 350-1000 m). The properties of the main water masses identified by *Gasparin et al.* [2014] at the entrance of the Coral Sea are also shown with bold black symbols. Oxygen saturation as a percentage is represented with black contours.

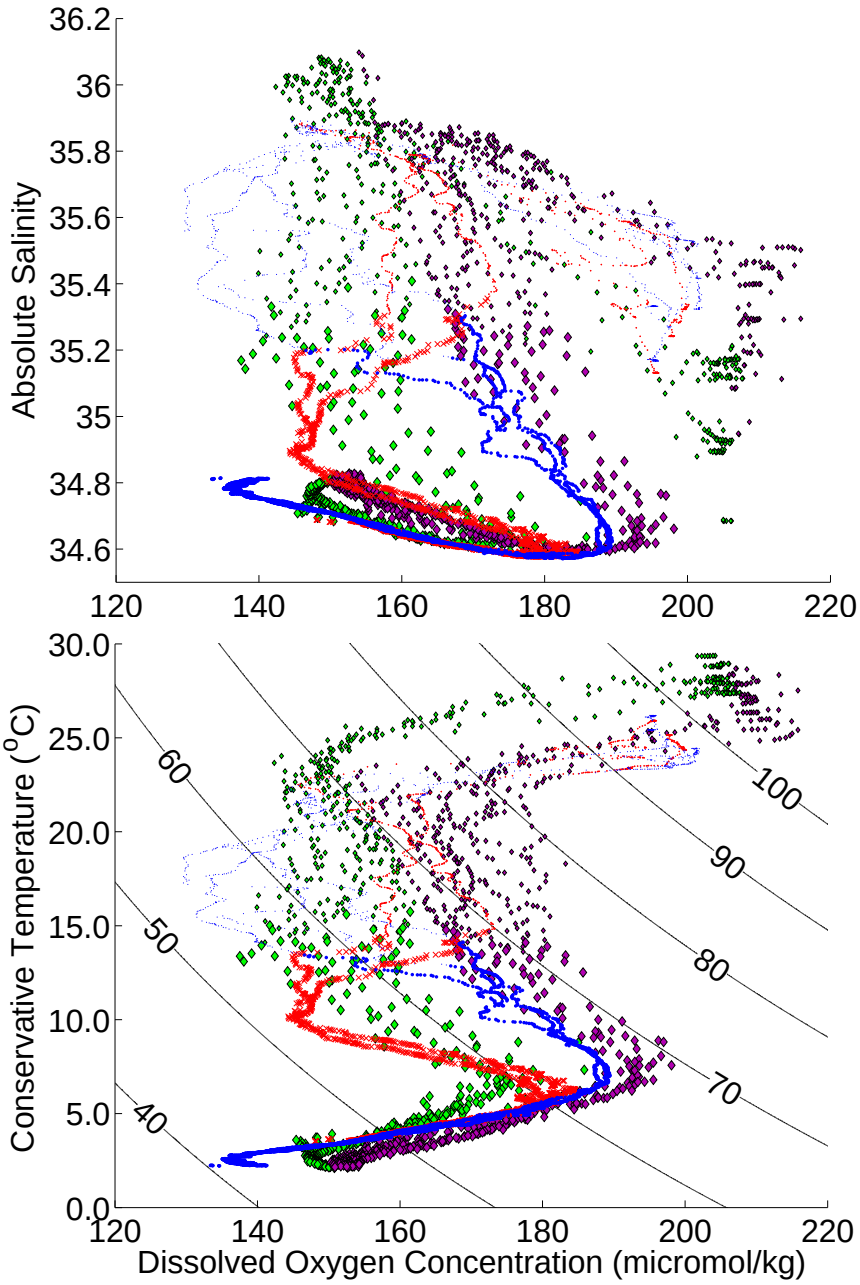

Figure 5. (a) Absolute salinity-Dissolved oxygen diagram for the CTD profiles and for the Argo float (WMO Id 5903381) profiles indicated in Figure 1.(b) Conservative temperature-Dissolved oxygen diagram for same data as (a). The upper part of the diagram is identified with small markers (layer 0-350 m) and the lower part is identified with big markers (layer 350-1000 m). Oxygen saturation as a percentage curves is represented with black contours.

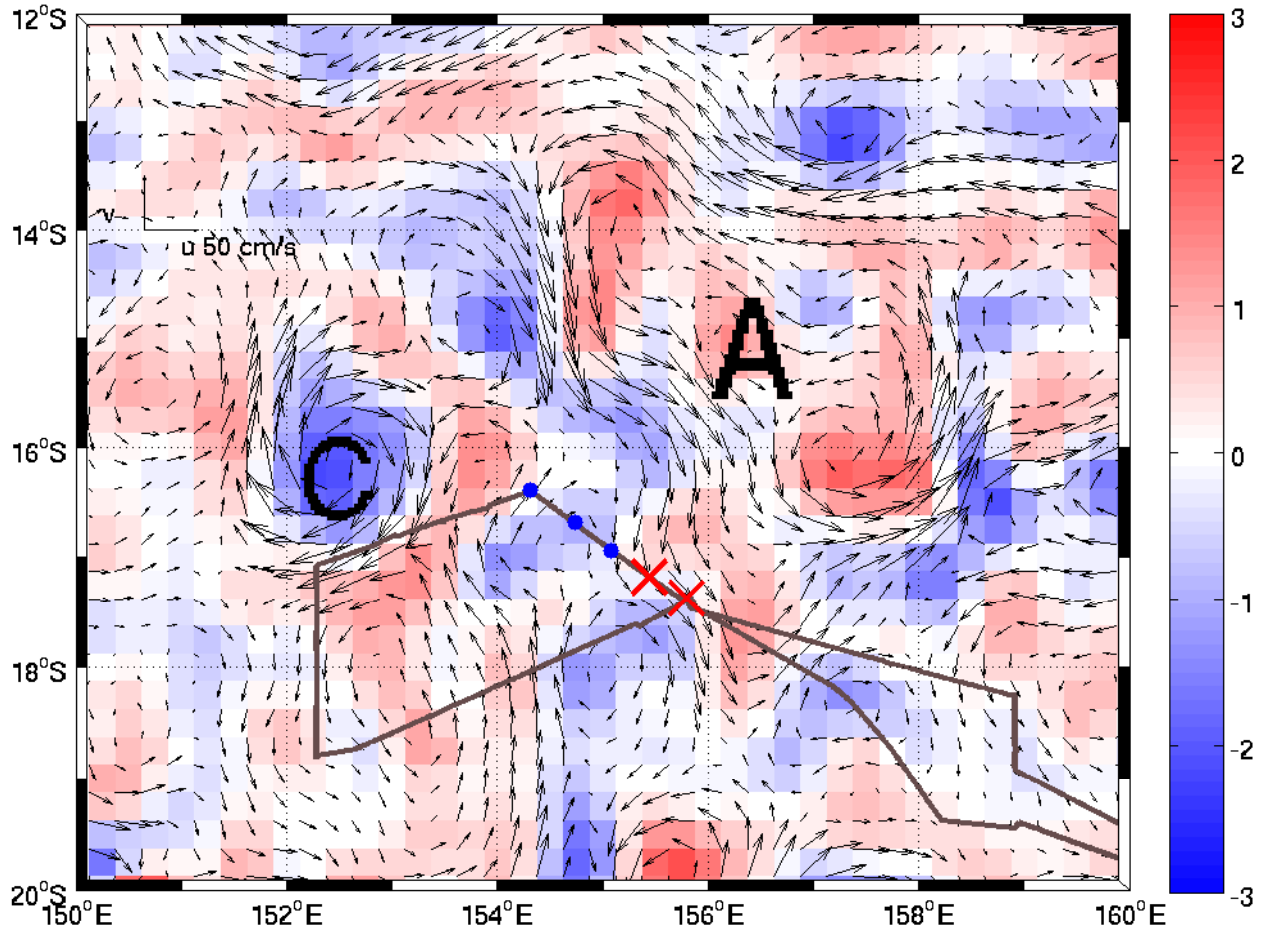

Figure 6. Relative vorticity [s^{-1}, colorbar] calculated using the AVISO absolute geostrophic currents on the 5 September 2012 (date when the CTD transect was sampled). Positions of the CTD-1 to 5 stations of interest are also shown.

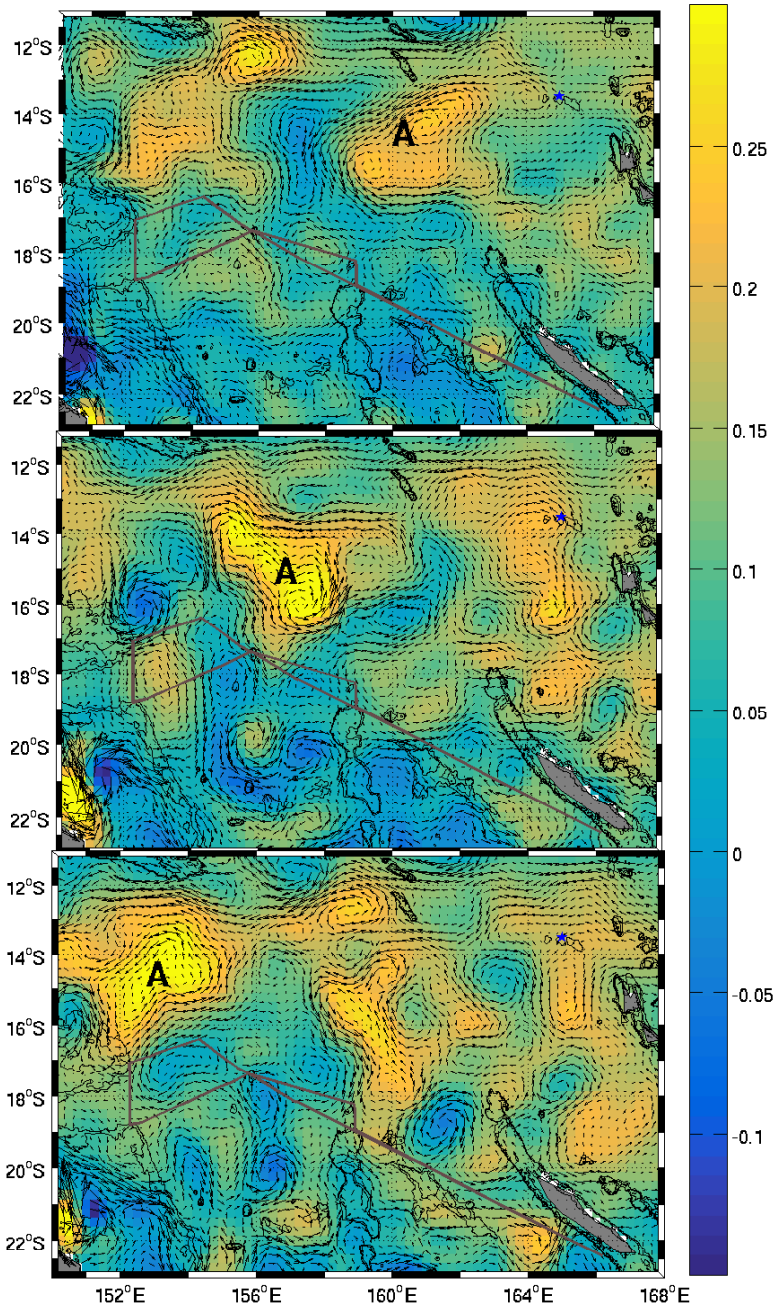

Figure 7. Daily sea level anomaly [m, colorbar] and absolute geostrophic currents [m s^{-1}] derived from AVISO data at the 1/4°horizontal resolution for 3 different dates (5 August, 5 September and 5 October 2012). The initial position of eddy A (1 August 2012) is shown with a blue star.

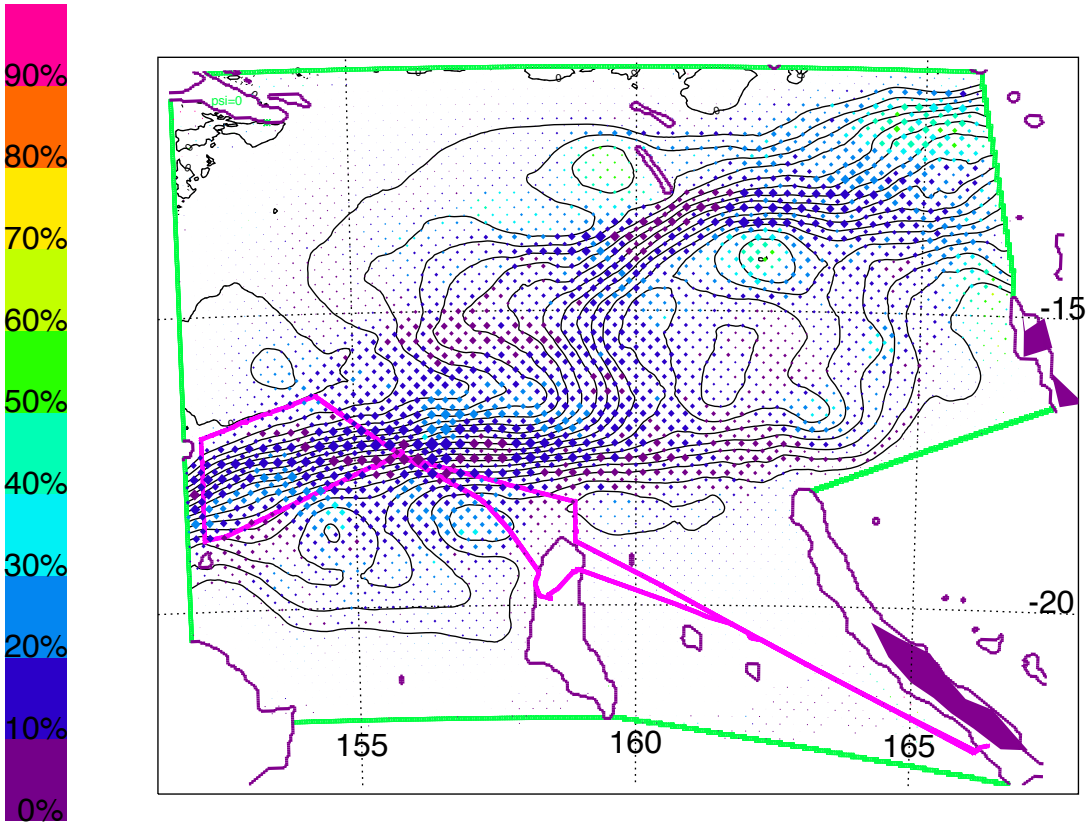

Figure 8. Lagrangian stream function calculated for the connection between the Ariane_NVJ and Ariane_SLI sections (black lines). The ratio between the transport deduced from the trajectory portions with a rotating behavior and the transport deduced from the full length of the trajectories is shown with diamonds. The color of the diamonds gives the intensity of this ration (in %), while the diamond size is proportional to the intensity of the local transfer. The green lines show the sections defined in Figure 1. Reef coasts, drawn in purple, are used to delimit sections.

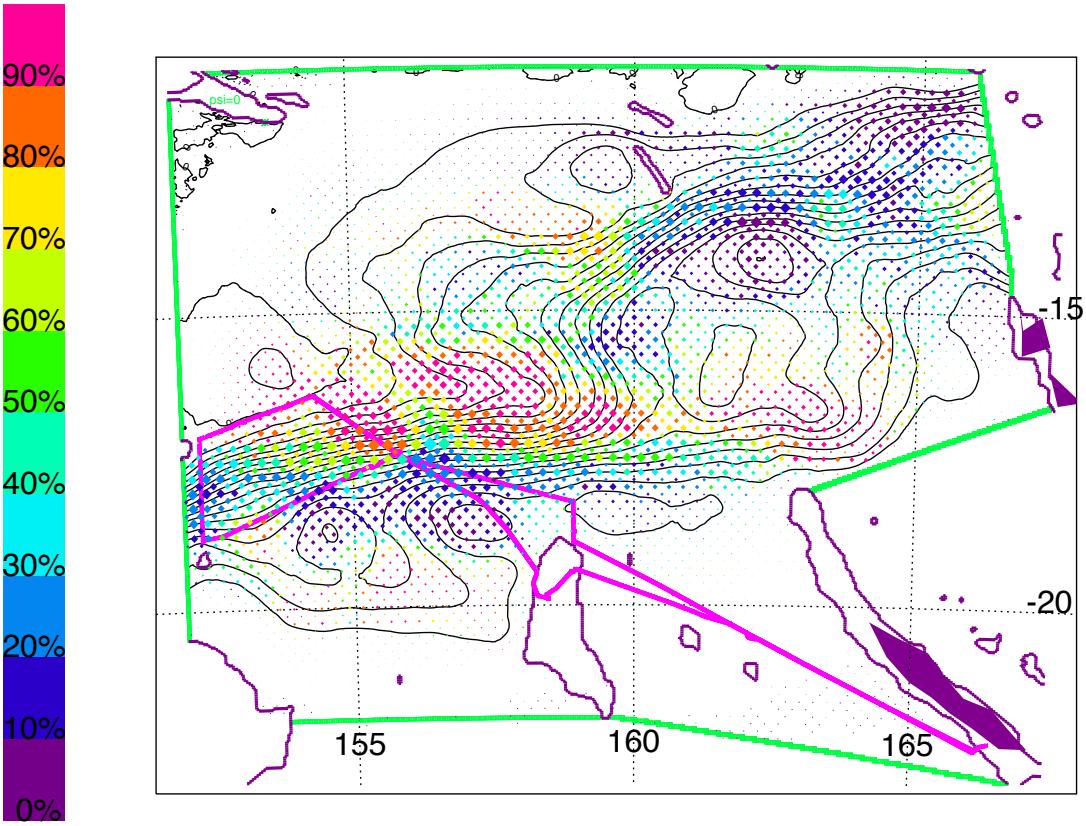

Figure 9. Same as in Figure 8 except for the colorbar that now shows the ratio (expressed in %) between the transport deduced from anticyclonic trajectory segments and the transport deduced from all the trajectory portions with a rotating behavior.